DIRECT NUMERICAL SIMULATION OF THE WAKE FLOW BEHIND A CYLINDER USING RANDOM VORTEX METHOD IN MEDIUM TO HIGH REYNOLDS NUMBERS

G. Heidarinejad and S. Delfani

Department of Mechanical Engineering, Tarbiat Modarres University
P.O. Box 14155-4838, Tehran, Iran, E-mail: gheidari@net1ef.modares.ir

(Recived: February 1, 1999 - Accepted in Final Form: May 1, 2000)

Abstract Direct numerical simulation of turbulent flow behind a cylinder, wake flow, using the random vortex method for an incompressible fluid in two dimensions is presented. In the random vortex method, the primary variable is vorticity of the flow field. After generation on the cylinder wall, it is followed in two fractional time step in a Lagrangian system of coordinates, namely convection and diffusion. No closure model is used and the instantaneous results are calculated without any *a priori* modeling. Regarding the Lagrangian nature of the method, there is a very good compatibility between the numerical method and physics of the flow. The numerical results are presented for a wide range of Reynolds number, 40-9500. In the initial stages, there is only an unstable symmetrical flow behind the cylinder and the vortex sheding is not started yet. But, in the high Reynolds number flows, two distinctive flow patterns, namely a and b are detected. The mechanism of generation of the primary and the secondary eddies can be related to the production, convection and diffusion of the vorticity field and the time dependent structure of the flow field in the wake zone behind the cylinder. The length of the computational domain, downstream of the cylinder, is selected 25 times of the cylinder's diameter. Regarding such a lengthy computational domain it is possible to detect the mechanism of generation, pairing and growth of the large scale structure, eddies. Although the instantaneous numerical results are calculated, no coresponding comparable results are available. Therefore, the validity of the results in this stage is only qualitative. For the quantitative comparison of the results, after the establishment of the stationary state, time averaged based indicators such as separation angle, drag coefficient, lift coefficient, Strouhal number and ... are calculated. The numerical results accurately fall within the range of the experimental measurements.

Key Words Cylinder, Wake, Turbulent Flow, Vortex, Random Walk, Lagrangian, Drag, Lift, Separation Angle

a°o{ ³¼§°ª ºB´¯B«p nj ³¯Ì±ŤWª Sz¸ o¼m¸B¯ ©½¼oU ¤B¼w ºkí¶ °j ¬B¼o] ºjkî ©¼¸Tv« ºpBw ³¼L{ **²k¼ña** ° £w±T« pk§±®¼n jªkîª nj »µjB~U ºBµ ³¶jo£ x °n pª ²jB´TWª B¶ »¯¿±¥ ºB´¯B«p nj ¬Ć Swj Ë¼½BQ q¼¯ ° S½oe ²nªk] º°n nj k¼§±U pª u¸ ³½ Swª ¤B¼w »Ť¼v¼Un° »¦æª o¼°T« ,»µjB~U ºBµ ³¶jo£ x °n nj /Swª ²k{ ³¾nª ¿B¶ ºo¼£»¸ -¦l±´¯ ° »½B\¶B]¦- o¶»½q] »¯B«p ¨B£ °j »¥ ºs¯½o£¿ RB~Ťh« ©Tv¼w ð½ nj B´Ć S½oe ,³¯Ì±ŤWª ³Ć¶ ³]±ÇU B¶ /j±{»« ³LwBd« ºpBw ¤k« ³¯±£_¼µ pª ²jB´TWª ¬°k¶ ° ºª³¨d§ Rn±æ ³¶ ¥æBe [½BT¯ /j±{¦»« ¤B¼Çw ¬B¼o] o¶ ©½¼Be »í¹ª° ¨q¼¯B¬« ° ¥æBe [½BT¯ Ë¼¶ »¶± i nB¼v¶ ºnB£pBw ,»¶BLwBd« x °n ¬j±¶ ºs¯½o£¿ /j±{»« ³¾nª ,¼4å-95åå ,pk§±®¼n jªkîª pª »í¼w° ³®«¼j ºko¶ ºjkî ºBµ¦ºpBw ³¼L{ pª¥æBe [½BT¯ /jnªj j±]° ²kz¯ pB±Ć p±®µ Bµ¦³¶jo£ éµj ° jnªj j±]° ¬nB¸Ť« nªk½BQB¯ »z ioa ³¼eB¯ £¸µ ³¯ª±ŤWª Sz¸ nj ³½ª ºB´¯B«p nj ºBµ¦³¶jo£ ¥¼ñzU ¨q¼¯Bñ« /Swª } ¼hzU ¥¶B¹ b ° a ºB´«B®¶ q½B²Ť« ¬B¼o] ²±¯° j ¿B¶ pk§±®¼n jªkîª nj B«ª Swª nªk½BQB¯ ¬B½o] nBT i Bw x oŤv£ ° ¸jB\¼ª B¶ ° ¤B¼w »Ť¼v¼Un° l±´¯ ° »½B\¶B] ,k¼§±U Ë¼¶ ¢BLUnª £w±U ³¼±¯BŸ ° ³½ª ³Ç¯±ŤWª o¤Ç¹ o¶o¶ 25 ,Swj Ë¼½BQ nj »UBLwBd« ¬ª k¼« ¤±¥ /j±{¦»« ¬B¼¶ ³¯ª±ŤWª Sz¸ nj »z ioa ·¼eB¯ nj ²k¼j »¶± i ³¶ Bµ³¶jo£ k{n ° ¬k{ S´] ,¥¼ñzU ¨q¼¯Bñ« »UBLwBd« ¬ª k¼« »£nq¶ ³¶ ³] ±U B¶ /Swª²k{ JBhŤª ¥¶B¹ ° ³¶Bz« o¼jB¸« B«ª k¯±{»« ³LwBd« ºª³¨d§ Rn±æ ³¶ ºjkî ºBµ ºpBw ³¼L{ pª¥æBe [½BT¯ ³ao£/j±{»« ³v½B¸« S´]¦³¶ /j±{»« ¨B\¯ª »´½ Rn±æ ³¶ ³¦eo« Ë¼ª nj RBLwBd« Sdæ ª¾m§ k{B¶»ª¯ Swj nj ºª³v½B¸« k®B« »½B´~ iB{ ,²k{ ºo¼£ £w±T« o¼jB¸« pª ²jB´TWª B¶ ,¤B¼w ¬B¼o] »Lv¯ ºnªk½BQ ºno¹o¶ pª u¸ , [½BT¯ »ª½ nj J±i nB¼v¶ S¹j B¶ ¥æBe [½BT¯ /k¯±{»« ³LwBd« /// ° ¤Bµ°oTWª jkî ,ko¶ K½o¡ ,Bv¸ K½o¡ ,»¼k] ³½°¼p /jo¼£»« no¹ »UBLwBd« [½BT¯ B½ »µB¢z½B«pĆ ºBµºo¼£ ²pªk¯ª²j°kd«

1. BACKGROUND

The unstable rotational flow of an incompressible fluid behind a cylinder has been subject of theoretical, numerical and

experimental study of many researchers. The first experimental study is attributed to Prandtl in 1925[1]. Apparently the most comprehensive experimental study is done by Bouard and Countanceau in 1980 [2]. Using the suspended color dyes in a special equipment, they obtained the pictures of almost instantaneous velocity profiles. However, they did not get the instantaneous values of quantities like drag coefficient or lift coefficients.

The nonlinearity of the governing Navier-Stokes equations is not the only difficulty in the numerical simulation of the flow in the range of medium to high Reynolds numbers. The numerical modeling of the flow in the recirculating zone behind the cylinder is also very difficult. As the Reynolds number increases, the instability of the flow also increases and a finer numerical mesh should be used which is accompanied by the other limitations.

For the turbulent flows, when the Reynolds number exceeds 2000, special remedies should be considered. Among the pioneers of the numerical simulation is the work of Payn, whose scheme was based on the finite difference method for the initial stages and for the range of Reynolds number 40-100[3]. His method was later used and complemented by other researchers and has been extended up to now [5].

The random vortex method was introduced for the first time in 1973 by Chorin [6]. Later in 1978, he presented the idea of vortex sheet and improved the accuracy of the results [7]. Later on, a lot of work has been done by other researchers which have been extended up to day [9].

In this work, not only the the unstable recirculating zone behind the cylinder is considered, but also in order to investigate the behavior of the large scale structures, eddies, in the later times, the length of the computational domain is extended for a much longer distance downstream of the flow field. In contrast to most other researchers whose computations are performed on the large mainframes or even super computers, in this work a lot of modifications and optimizations are done to run the code on personal computers.

2. INTRODUCTION

Numerous efforts have been concentrated on the numerical simulation of the flow around the cylinder; one of the most important of which is the random vortex method. In this method, the vorticity field is discretized into a finite number of vortex element with the specified strengths. Lagrangian nature of the random vortex method is compatible with the governing mechanisms of the flows and the accuracy of the numerical results falls within the range of the experimental measurements. Regarding the flow around a solid body, it is possible to interpret the process of the formation of the primary and the secondary eddies in accordance with the Navier-Stokes equations. To satisfy the no-slip condition, the vortex sheets are generated on the external surface of the cylinder which are displaced downstream via the mechanisms of diffusion and convection. Pairing of the vortices leads to the formation of the primary and the secondary eddies behind the cylinder. Passage of the eddies with different size and strength over a fixed point, is responsible for the apparently random induced velocity.

In the random vortex method, track of a finite number of vortex elements are kept in a Lagranginan reference of frame. The value of the velocity at the center of each element is a function of the position and the strength of all

other elements. Each time step is divided into two fraction steps. In the first fractional time step, the mechanism of diffusion is frozen and displacement of the center of elements which is due to convection of the flow field are calculated using a fourth order Runge-Kutta integrating scheme. In the second fractional time step, the effect of diffusion is considered using a random walk. In vortex method, as time step decreases, although the number of computational elements increases, the numerical results converge to the experimental measurements and hence the division of time step into two fractional steps is justified [13]. Regarding the tracking of the vortices in a Lagrangian reference of frame, it is, a time dependent, no-closure model and a grid free computational method. Instead of the primary variables, such as the velocity and pressure, the secondary variable namely vorticity is used.

3. GOVERNING EQUATIONS AND THE NUMERICAL SCHEME

3-1 The Governing Equations The governing equations for the incompressible fluid in two dimension are:

$$\hat{e}.\mathbf{u} = 0 \tag{1}$$

$$\frac{\tilde{A}\mathbf{u}}{\tilde{A}t} + \mathbf{u}.\hat{e}\mathbf{u} = - \hat{e}p + \frac{1}{Re} L\mathbf{u} \tag{2}$$

$$\mathbf{u} = 0 \quad \text{on Boundary , } (\tilde{A}D) \tag{3a}$$

$$\mathbf{u} = 0 \quad \text{in time } t = 0 \tag{3b}$$

where Equations 1 and 2 experss the conservation of mass and linear momentum while Equations 3a and 3b represent the boundary conditions and the initial condition respectively. In these equations, u and v are components of the velocity vector **u** in the x and y directions and p is the pressure. Values of u, v and p are non-dimensionalized with respect to the free stream velocity of the fluid around the cylinder, V and $\frac{1}{2}\rho V^2$ accordingly. Also the real time, t, is non-dimensionalized with respect to V/2R where "R" is the radius of the cylinder. The other symbols, namely Reynolds number, Laplacian and the gradient are defined as follows:

$$Re = \frac{\rho V(2R)}{\mu}$$

$$L = \frac{\tilde{A}^2}{\tilde{A}x^2} + \frac{\tilde{A}^2}{\tilde{A}y^2}$$

$$\hat{e} = \frac{\tilde{A}}{\tilde{A}x}\mathbf{i} + \frac{\tilde{A}}{\tilde{A}y}\mathbf{j}$$

By taking curl of Equation 2, the transport equation of vorticity is obtained in which the pressure term is absent.

$$\frac{\tilde{A}w}{\tilde{A}t} + \mathbf{u}.\hat{e}w = \frac{1}{Re} Lw \tag{4}$$

$$w = \frac{\tilde{A}v}{\tilde{A}x} - \frac{\tilde{A}u}{\tilde{A}y} \tag{5}$$

In reality, the transport of vorticity, is due to the simultaneous effects of mechanisms of convection and diffusion. But, because of the smallness of the computational time step, it is possible to divide Equation 4 into two equations, namely, 6 and 7. Or, each computational time step is divided into two fractional steps and each of the mechanisms of convection and diffusion affect the flow field in the absence of the other.

$$\frac{Dw}{Dt} = \frac{\tilde{A}w}{\tilde{A}t} + \mathbf{u}.\hat{e}w = 0 \tag{6}$$

$$\frac{\tilde{A}w}{\tilde{A}t} = \frac{1}{Re} Lw \tag{7}$$

3-2 Convection Using the definition of the velocity component, u and v, in terms of the stream function, ψ, the continuity Equation 1 is satisfied. Substituting the definitions in Equation 5, will result in the Poisson's equation

$$u = \frac{\tilde{A}\psi}{\tilde{A}y}, \quad v = -\frac{\tilde{A}\psi}{\tilde{A}x},$$

$$L\psi = - w(\mathbf{x}) \tag{8}$$

The solution of this equation in a free space is a Green function:

$$y(\mathbf{x}) = G(\mathbf{x}-\mathbf{x}'')\, w(\mathbf{x}'')\, d\mathbf{x}'' \quad (9)$$

$$G(\mathbf{x}) = \frac{-1}{2\pi} \mathrm{Ln}(r)$$

In this relation r is the distance between the origin of the system of coordinate and the center of the vortex element, $d\mathbf{x}''=dx''dy''$ is the area of the element and $G(\mathbf{x})$ is the Green function.

In the random vortex method, the vorticity field is considered in terms of summation of vortex elements. The contribution of the vorticity around each element is in accordance with a radially symmetric function, i.e. core function f_σ, where σ is the core radius of the element. Therefore, the vorticity distribution due to all vortex elements is as follows:

$$w(\mathbf{x}) = \sum_{i=1}^{n} \Gamma_i f_\sigma(\mathbf{x}-\mathbf{x}_i) \quad (10a)$$

$$f_\sigma = \frac{1}{\sigma^2} f\left(\frac{z}{\sigma}\right) \quad (10b)$$

$$f(z) = \begin{cases} \frac{1}{2\pi z} & z \geq 1 \\ 0 & z<1 \end{cases}$$

where n, f_σ and Γ_i are the number of vortex elements, core function and the strength of the elements respectively. Therefore, the induced velocity - due to the vorticity - in each arbitrary point in the flow field is calculated as follows [14]:

$$\mathbf{u}(\mathbf{x}) = \sum_{i=1}^{n} \Gamma_i K_\sigma(\mathbf{x}-\mathbf{x}_i) \quad (11a)$$

$$K_\sigma(\mathbf{x}) = \frac{-1}{2\pi} \frac{(y,-x)}{r^2} k\left(\frac{r}{\sigma}\right) \quad (11b)$$

$$k(r) = \begin{cases} r & r \geq 1 \\ 1 & r>1 \end{cases} \quad (11c)$$

$$r = |\mathbf{x}-\mathbf{x}_i| \quad (11d)$$

Knowing the velocity in the center of elements, the displacement due to the mechanism of convection in each time step is computed.

3-3 Diffusion The transport of vorticity field due to diffusion is in accordance with Equation 7. In the random vortex method, the contribution of this mechanism is considered as a statistically Gaussian distribution [15,16]. Regarding similarity of the Gaussian distribution with the solution for the diffusion effects, each vortex element is given a random displacement in x and y directions, i.e. m_x and m_y with the standard deviation of $L_{st}= \sqrt{\frac{2\,\Delta t}{\mathrm{Re}}}$ and zero mean. The mentioned random values are calculated as Kloeden [17]. Therefore, the total effect is due to diffusion and convection in each time step which are calculated as follows:

$$x_i(t+\Delta t) = x_i(t) + u_i \Delta t + m_x \quad (12a)$$

$$y_i(t+\Delta t) = y_i(t) + v_i \Delta t + m_y \quad (12b)$$

where m_x and m_y are two independent random values. In Equation 12, both u_i and v_i are made of two part. The first part is the velocity induced by the other vortex elements and their images i.e. u_w, u_{wi} and v_w, v_{wi} known as Biot-Savart law which is calculated by Equation 11a accordingly. The second part is the velocity due to the effect of the boundary conditions on the solid walls and the distance from the cylinder, which is a velocity due to a potential. Calculation of the latter part is presented below.

3-4 Boundary Condition On the solid wall, both the normal and tangential velocity should be identically zero.

$$\mathbf{u}.\mathbf{n} = 0 \qquad \text{on the boundary } (\partial D)$$
$$\mathbf{u}.\mathbf{s} = 0$$

where $\mathbf{n}$ and $\mathbf{s}$ are unit vectors normal and tangent to the wall.

Imaging method is used to make the normal component of the velocity zero [18,19]. For the vortex element at a distance r from the center

of the cylinder, two images should be considered. The first one in the distance R^2/r and with the opposite sign of the main vortex, and the other with the same sign but in the center of the cylinder. The induced velocity due to both images, u_{wi} and v_{wi}, are calculated in accordance with Equation 11a).

In order to satisfy the no-slip condition on the solid wall, vortex sheets are employed. These vortices are initially generated on the solid boundary. Later, due to the diffusion effects, they are separated from the solid wall and are moved inside the flow field. Within the distance D_s from the solid wall, vortices are sheet type and beyond that they are considered as blob type [16,20].

In order to establish the boundary condition far from the cylinder, the velocity due to a potential, u_p and v_p, are considered. Therefore, the components of the total velocity in arbitrary points, u and v, are as follows:

$$u = u_p + u_w + u_{wi} \quad (13a)$$

$$v = v_p + v_w + v_{wi} \quad (13b)$$

where u_p, v_p, u_w, v_w, u_{wi} and v_{wi} are velocities due to the potential, vortex element (both sheets and blobs) and images of the vortex element (both sheets and blobs). Both u and v are used in equations (12a and b) to calculate the values of $x(t + Dt)$ and $y(t + Dt)$ respectively.

3-5 Vorticity Distribution within the Vortex Sheet If a vortex is within the distance D_s from the solid wall, it should be of sheet type and distribution of the vorticity around it is considered as follows:

$$w(\mathbf{x}) = \sum_{i=1}^{n} \int \gamma_i f_L(\mathbf{x}-\mathbf{x}_i)\, d\mathbf{x} \quad (14)$$

$$f_L(x) = \frac{1}{h}\, \delta(y) \left\{H\left(x + \frac{h}{2}\right) - H\left(x - \frac{h}{2}\right)\right\} \quad (15)$$

where $\delta(y)$ is Dirac delta function, H(x) is the Heavy side function, h is the length of sheet and γ_i is the strength of the sheet respectively.

4. NUMERICAL SCHEME AND THE MEAN DRAG AND LIFT COEFFICIENT

4-1 Steps Different steps of the numerical algorithm are as follows:

(a) Perimeter of the cylinder is divided into m segments and the induced tangential velocity in the center of each segment is calculated. The value of the induced velocity is assigned as the strength of the vortex sheets in that segment. This value is compared with the maximum allowable strength for each sheet, i.e. Γ_{max}, and an integer number of sheets with the strength less than that are generated.

(b) The induced velocity due to the other elements in the center of the sheet is calculated.

(c) Using the random walk method, the displacement due to diffusion is calculated.

(d) Using Equations 13a and 13b, the total velocity for each vortex is calculated.

(e) Using the Relations 12a and 12b, all vortex elements are moved to the new location.

(f) In order to keep the computation volume within the applicable range and drop the less important vortex elements, downstream and beyond the 25 times of the cylinder's diameter, all vortices are deleted. If a vortex element falls inside the cylinder, it is also deleted.

(g) Of course, in the new situation, the no-slip condition is not satisfied any more. Therefore, in accordance with step (a) above, the velocities at the center of segments are calculated again and steps (b) through (g) are repeated.

4-2 Calculation of the Coefficient of Drag and Lift The drag and lift forces are generated from two sources. The first, is the viscous forces due to the effect of fluid on solid walls, and the other is due to the net effects of pressure from

the fluid to the body surface. Knowing the coefficient of each force, the value of that force can be calculated.

(a) Darg coefficient

$$C_D = (C_D)_m + (C_D)_p \quad (16)$$

where, $(C_D)_m$ and $(C_D)_p$, are drag coefficients due to viscous and pressure effects which are calculated as follows:

$$(C_D)_m = \frac{-1}{Re}\int \omega_{\tilde{A}} \sin\theta \, d\theta \quad (17a)$$

$$(C_D)_p = \int p_{\tilde{A}} \cos\theta \, a \, d\theta \quad (17b)$$

(b) the lift coefficient

$$C_L = (C_L)_m + (C_L)_p \quad (18)$$

where, $(C_L)_m$ and $(C_L)_p$, are the lift coefficient due to viscous and pressure effects and are calculated as follows:

$$(C_L)_m = \frac{-1}{Re}\int \omega_{\tilde{A}} \cos\theta \, d\theta \quad (19a)$$

$$(C_L)_p = \int p_{\tilde{A}} \sin\theta \, a \, d\theta \quad (19b)$$

In Relations 17 and 19, $\omega_{\tilde{A}}$ and $p_{\tilde{A}}$ are the values of vorticity and pressure on the perimeter of the cylinder and all integrations are performed numerically. The instantaneous values of the coefficient of drag and lift are calculated for the different Reynolds numbers and after time averaging, the mean values are compared with the experimental measurements.

5. RESULTS

In this study, the number of segments on the perimeter of the cylinder is selected 20 to 40 and the maximum allowable strength of elements is limited to Γ_{max}=0.25. The value of time step, Δt, in the initial times, i.e. $t \leq 3$, is assumed to be 0.03 while for the later times its value is chosen 0.1. Value of D_s is also calculated from Equation 20

$$D_s = 0.037\,\pi\,Re^{-\varphi} \quad (20)$$

More details about Equation 20 is addressed to reference [20]. Due to the adverse pressure gradient behind the cylinder and after separation point, the fluid separates, and a wake flow results which generates two symetric eddies. The strength of these eddies depends on the value of Reynolds number. At $Re < 40$, the inertial effects are small and hence these eddies are attached to cylinder and remain stable.

When the Reynolds number of the flow exceeds 40, the flow around the cylinder is divided into two parts:

(a) stable situation in the initial stage, during which two main symmetric eddies begin to generate and grow. At this stage, because of the weakness and incomplete growth of eddies, there is not enough inertia, velocities are small and, hence, they remain attached to cylinder and keep their symmetry.

(b) unstable situation in the later times, $t \geq 3$, during which because of the growth of eddies, velocity in recirculating zone increases. One of two eddies, which is closer to cylinder, remains unchanged while the other continues to grow. As soon as this eddy detaches from the cylinder and moves downstream, the other eddy which is closer to cylinder begins to grow. Meanwhile, a new eddy is born which fills the vacancy of the former eddy and follows the same pattern. The latter eddy continues to grow, eventually detaches and moves downstream, together forming vortex street. This process induces a higher velocity in the recirculating zone.

5-1 Structure of flow in Re = 3000

5-1-1 Stable State in the Initial Stage The main point in the stable state is generation of the primary symmetric eddies and formation of a and b structures. As Reynolds number increases, $500 > Re > 40$, primary eddies grow, velocity increases, and leads to a recirculating

zone. A new (secondary) eddy begins to form close to the cylinder wall, rotating in the opposite direction of the primary eddies. This process is responsible for the formation of a structures a structure- After tÂ1.5 and when the primary eddy is stable in the upstream, as Reynolds number increases, Re> 500 , the previously mentioned secondary eddy grows and generates another symetric eddy close to the cylinder wall, and hence a region forms, which

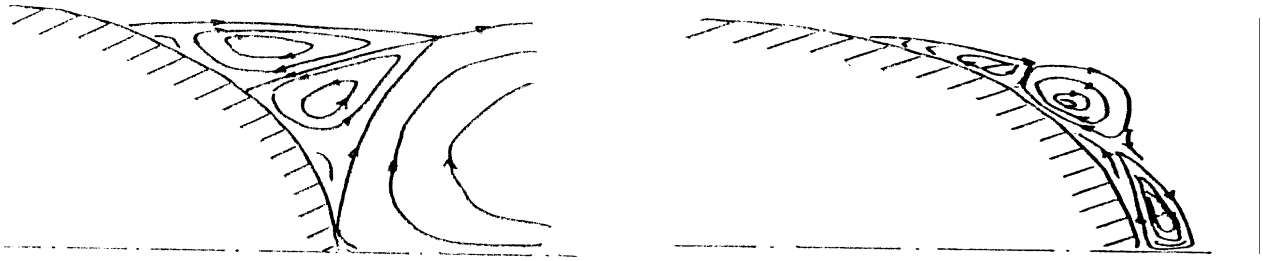

(a) (b)

Figure 1. (a) a structure (b) b structure /

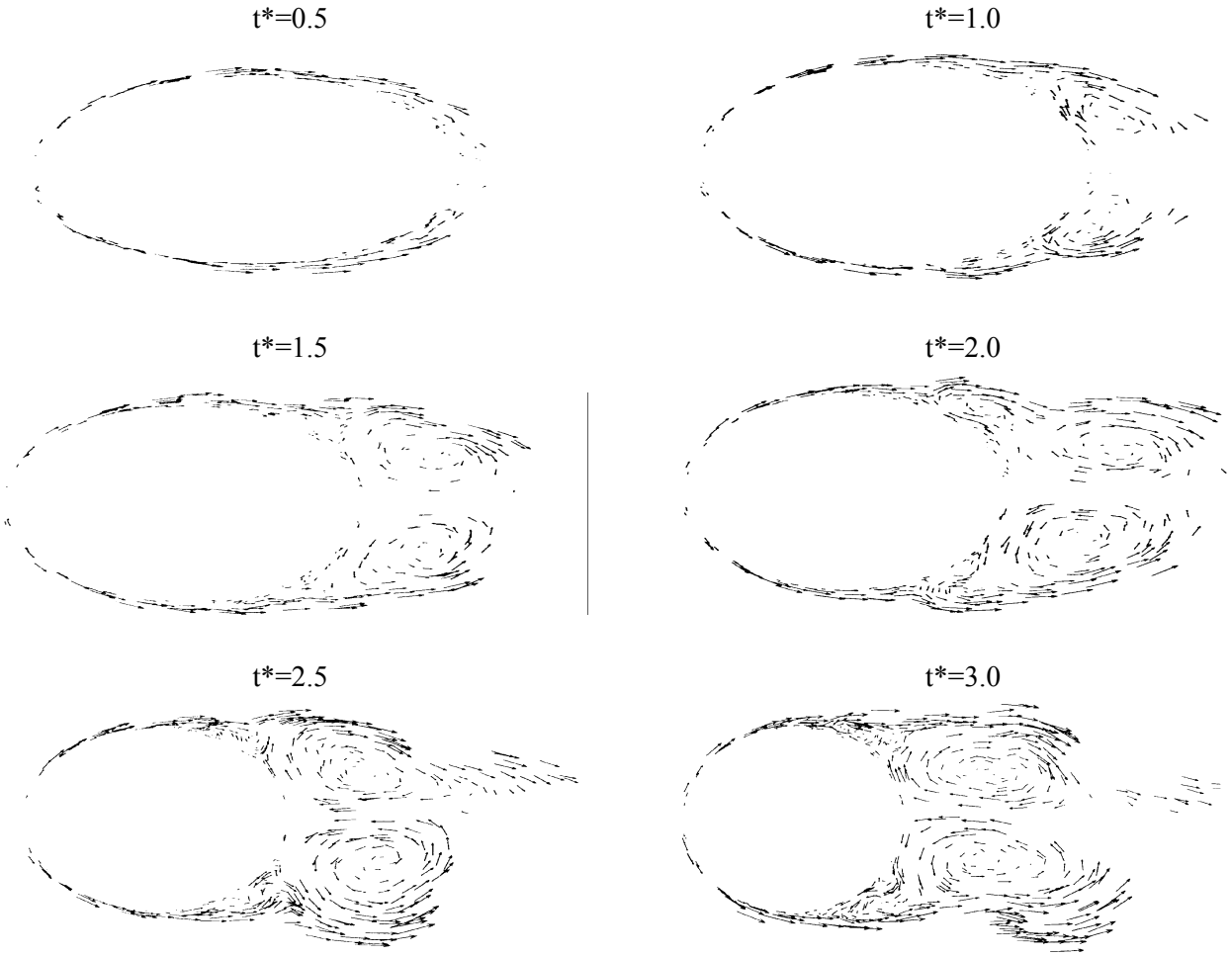

Figure 2. Positions and velocities of vortex elements during t<3.0 at Re=3000.

contains two symmetric eddies, shown in Figure 1a.

In Figure 2 the position and velocity vector of all vortex elements during times 0.5-3 are shown. It is clear that a secondary eddy is present in t= 1.5, and because of the high velocities in the recirculating zone, another secondary eddy in the symmetric position with

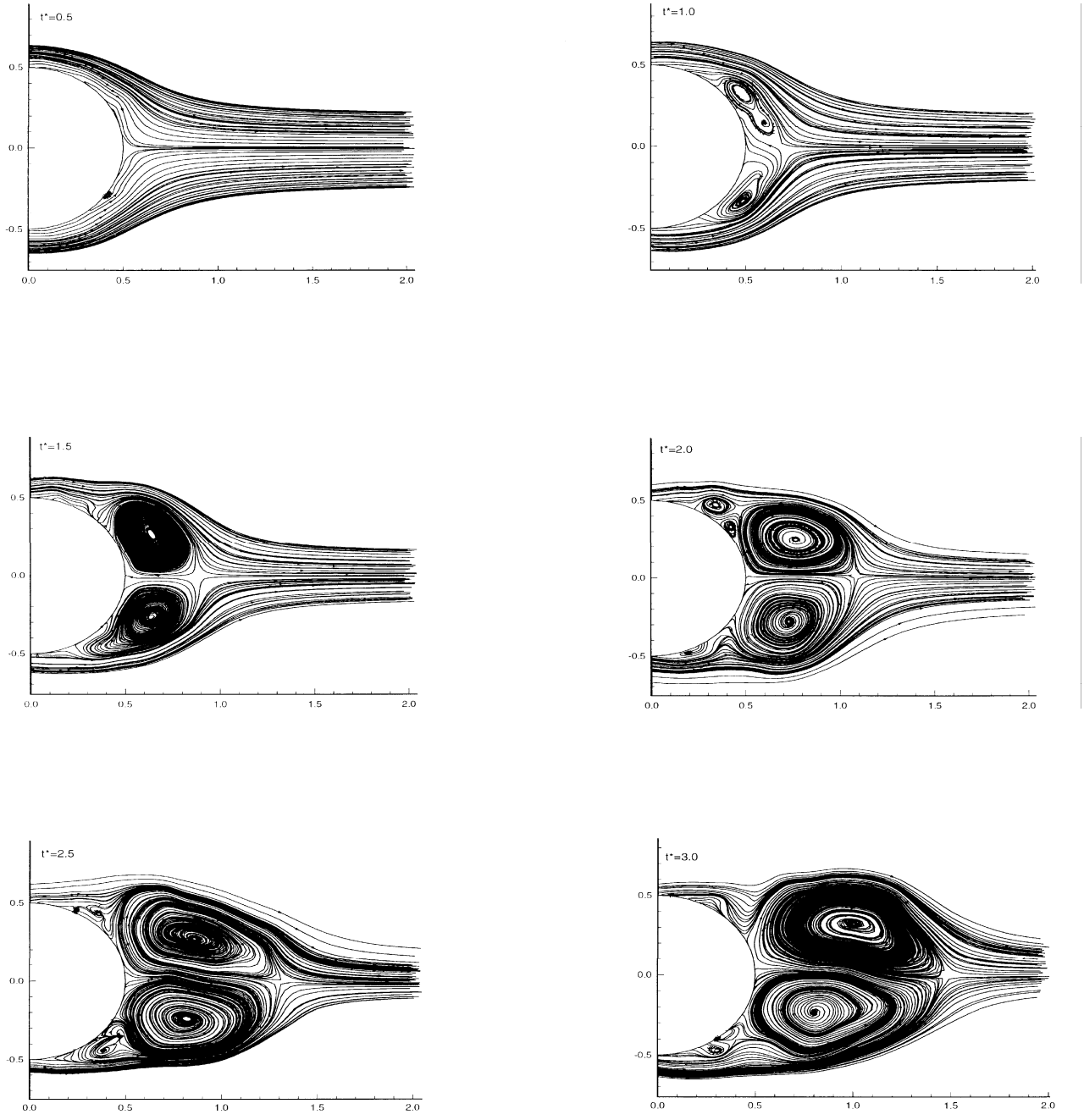

Figure 3. Streamlines for a structure during t<3.0 at Re=3000.

respect to the first one is born.

In Figure 3 the streamlines behind the cylinder are shown in which the mentioned mechanism is better seen b structure - Before tÀ1.5, preceding to a structure, the b structure happens whose schematic structure is shown in Figure 1b. At t= 0.5, a tiny recirculating region close to the cylinder forms. Core of this region which locates in the most negative vorticity zone, goes through a fast rotation. Around time t=1 a new eddy forms which is going to become a primary eddy. At t= 1.5, the process is complete and a structure begins to form. In Figures 2 and 3, formation of b structure is clearly depicted.

In Figure 4 the variation of the radial velocity on the symmetric axis of the recirculating zone in different times is shown and compared with the experimental measurements in reference [2]. The comparison shows the high accuracy of the results. It is clear that the value of v/v_0 at t=3 begins to oscillate, indicating the formation of a passage for eddies, which shows the same physics of flow.

The region with negative value of v/v_0 is the recirculating zone. As time goes on, the recirculating zone and the primary eddy grow, and the induced negative velocity increases.

Also in Figure 5 time dependent $-(u_{max})/v_0$ and d/2R, where "d" is the location of $-u_{max}$, is plotted. By the same reasoning above, it is clear that the most negative velocity will happen farther downstream. At time t< 1, the value of $-(u_{max})/v_0$ increases smoothly, but at 1< t< 2.5, the rate of its change increases. Finally at t>2.5 the rate of change decreases. Therefore, an extremum point can be considered at t= 1.7. Also at t=3 the value of $-(u_{max})/v_0$ is almost 1.4, indicating strength of eddies in the recirculation zone. Also, the value of "d" increases linearly in a well organized manner. Both curves indicate very good agreement with the experimental measurements [2,8].

In Figure 6 time dependent length and width of the main eddy center, "a,b", and length of the recirculating zone, "l", are plotted. In this figure displacement of the center of eddies are quite clear. At t< 0.9 the value of "a" is negative, indicating that the growth of eddy is not complete. As time increases, the value of "a" also increases. Also the value of "b" decreases, indicating a fundamental difference between this flow and the flow at the lower Reynolds number.

In Figure 7 the separation angle versus time is plotted. Results are compared with the This leads to cyclic separation of eddies from the cylinder, sheding downstream and forming

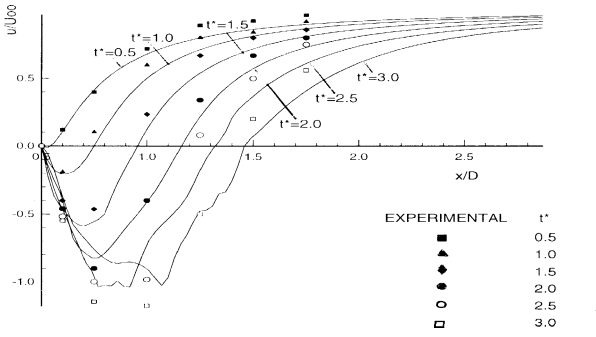

Figure 4. Radial velocity on the symmetric axis.

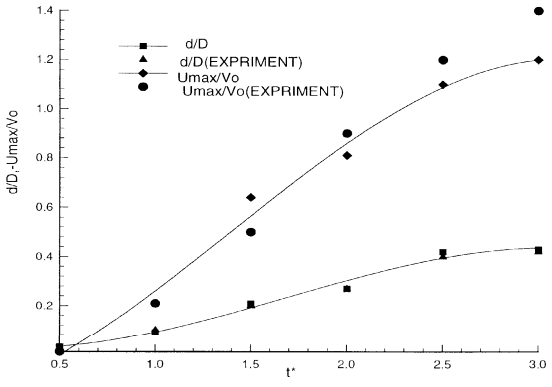

Figure 5. Location of u_{max} versus time

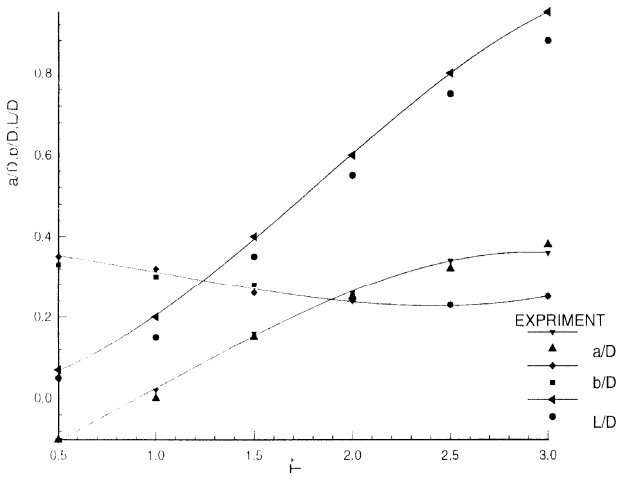

Figure 6. Length and width of eddies versus time.

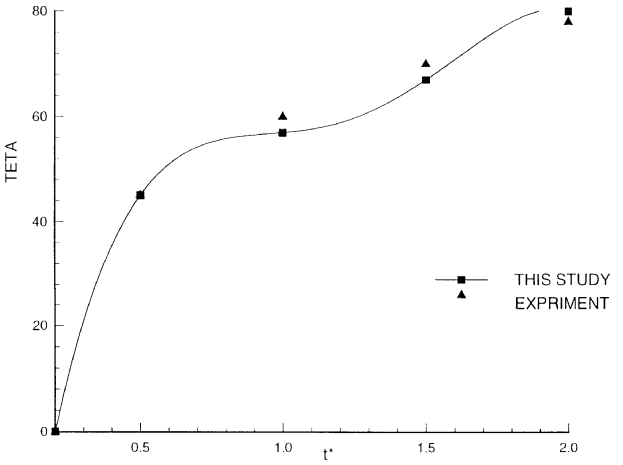

Figure 7. Separation angle versus time.

experimental measurements [6].

5-1-2 Unstable State in the Later Times After tÂ3 the geometry of flow becomes asymmetric. the wake zone. In Figure 8 the time dependent drag coefficient of the cylinder with time is presented. Under the influence of cyclic movement of eddies, fluctuation of separation angle and the gradient of velocity, the value of the drag coefficient changes with time.

All mentioned parameters are also responsible for the fluctuation of lift coefficient. In Figure 9 the variation of the lift coefficient versus time is plotted.

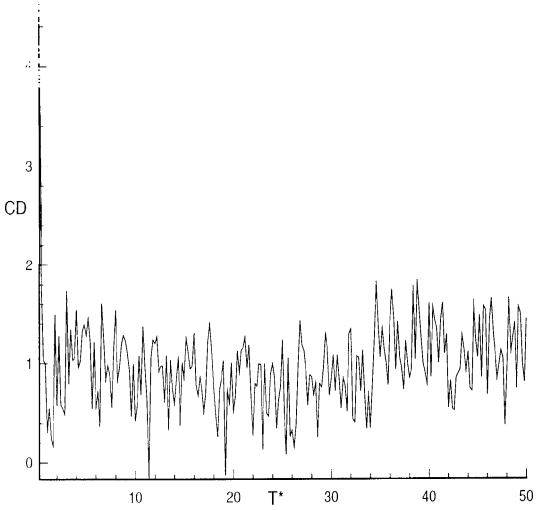

Figure 8. Drag coefficient versus time.

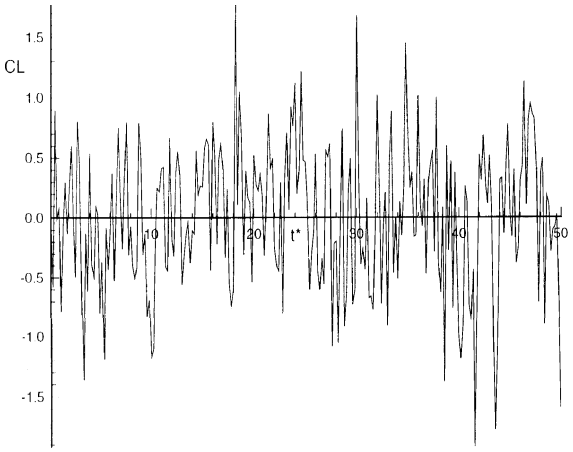

Figure 9. Lift coefficient versus time.

In Figure 10 streamlines of the flow behind the cylinder are plotted. It is clear that there is a repeated situation between times t= 20.5 and t= 25. The corresponding Strouhal number is 0.21-0.22 which falls within the range of the experimental measurements.

In Figure 11 the location and velocities of the vortex elements downstream of the cylinder in the range of t=29 to t=35 are plotted.

5-2 Structure of flow in Re=9500

The structure of this flow is similar to that of the flow at Re= 3000, except, at t> 2 the flow becomes unstable and the wake zone begins.

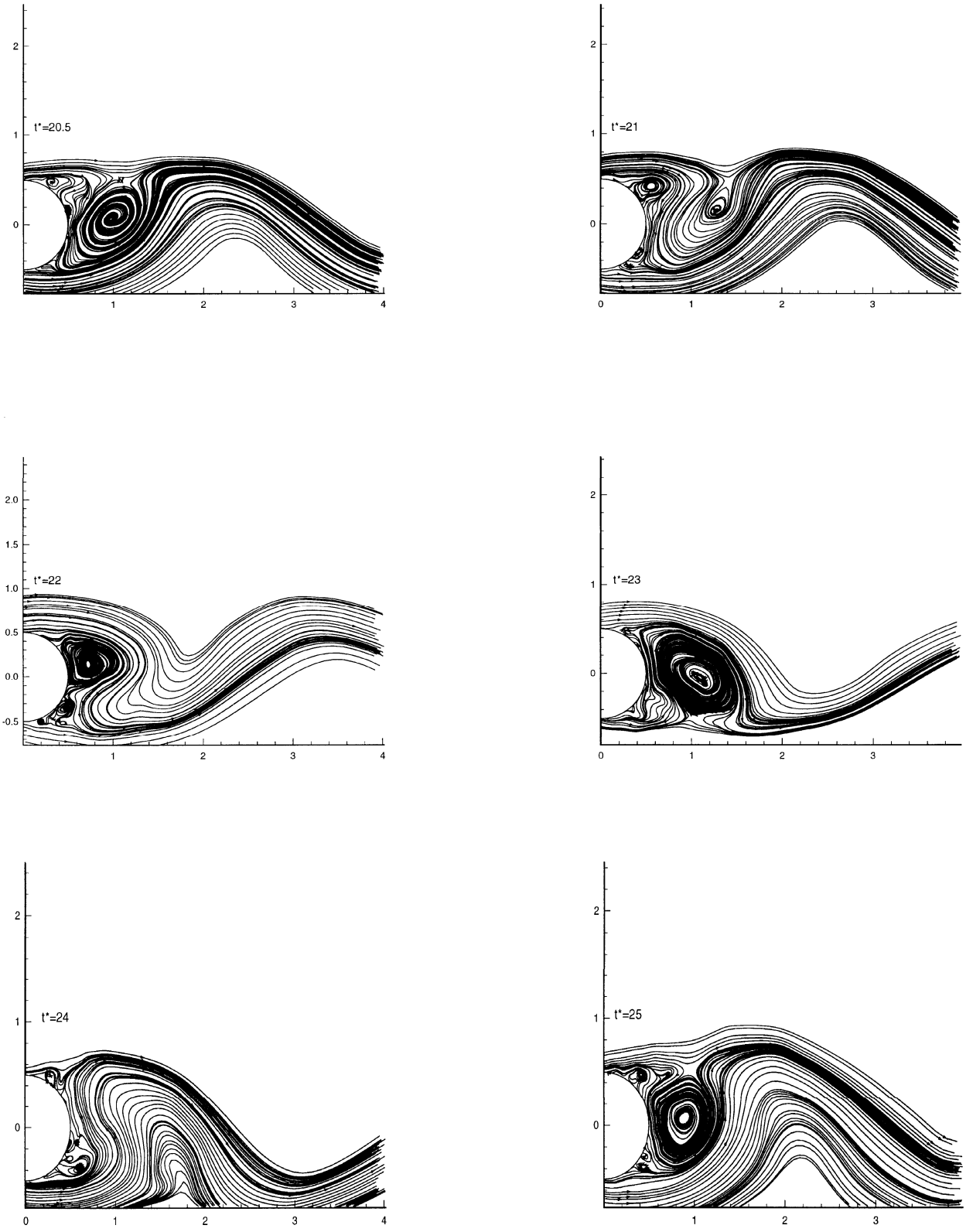

Figure 10. Streamlines of flow at later time, t=20.5 to t=25.

Figure 11. Positions and velocities of vortex elements downstream versus time at Re=3000.

For the initial times, $t < 3$, the location and velocity of the vortex element are plotted in Figure 12. In Figure 13 the streamlines for the same period of time are presented.

The a and b structures and the asymetry of the main eddies are better pronounced than the flow with Re= 3000. The graphs showing the geometrical properties of the flow are presented in Figures 14, 15 and 16. Explanation and interpretation of these figures are the same as that at Re = 3000. All of the numerical results show good agreements with the experimental measurements. In Figure 15, because of the higher value of Reynolds number, and increase of instability, the accuracy of results decreases slightly. This can be improved by decreasing the value of time step and increasing the number of computational elements.

In Figure 17 the variation of drag coefficient with Reynolds number is presented which is also

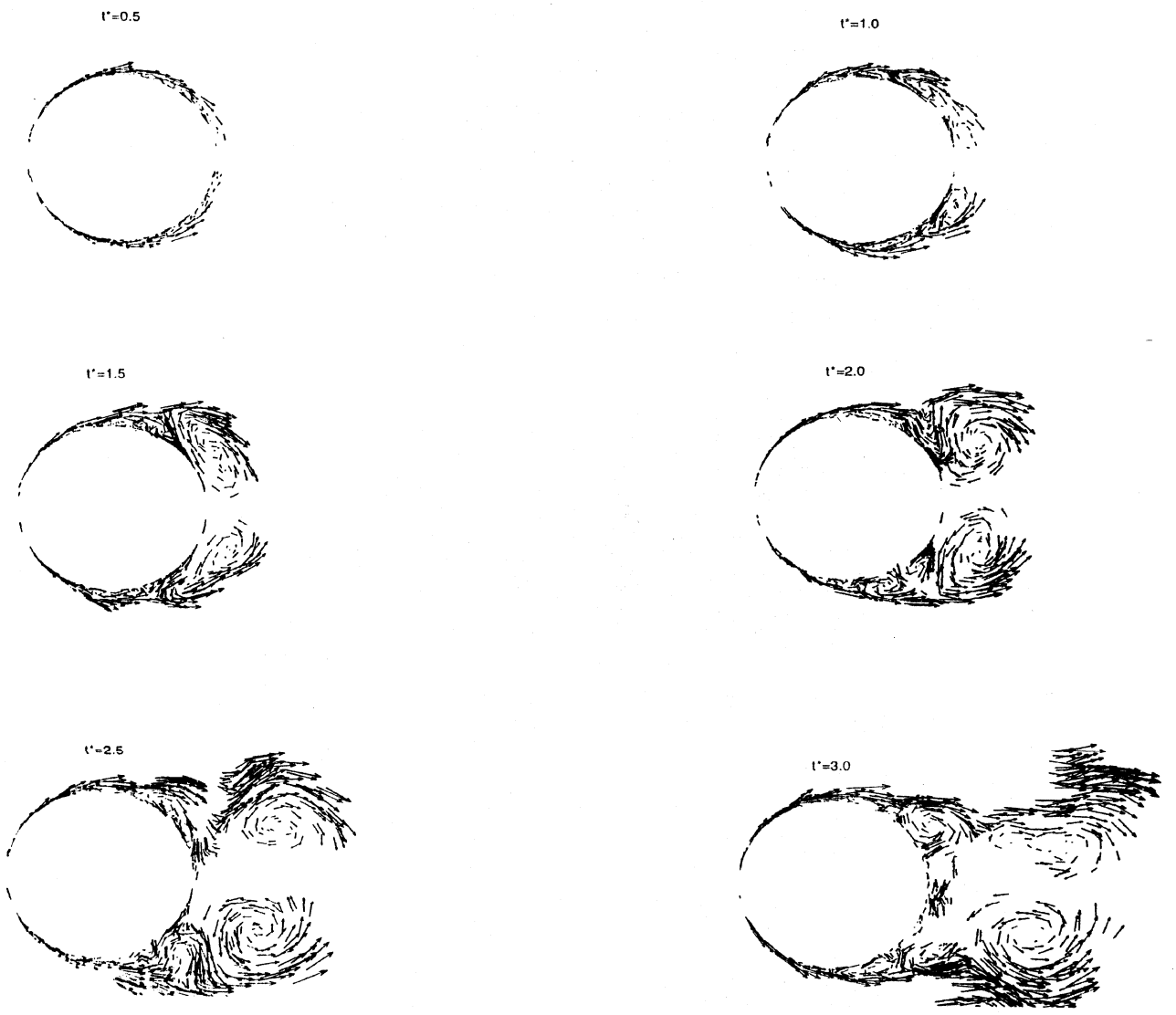

Figure 12. Positions and velocities of vortex elements during t<3.0 at Re=9500.

compared with the experimental measurements. As it is noticed the accuracy of the results is remarkable.

For the unstable flow, variation of the coefficients of lift and drag are presented in Figures 18 and 19.

In Figure 20 the streamlines for time interval 20.5 - 25 are plotted.

At last, Figure 21 is presented in which the location and velocities of the vortex elements for time interval of 30 - 45 are plotted.

Usually the results presented in Figures 11 and 21 can not be obtained by other researchers using the experimental methods because, their setups are not capable of handling such long times. In these figures the mechanisms of formation, pairing, growth and the motion of eddies to downstream of the flow field are clearly seen. Although extending the computational domain to downstream is

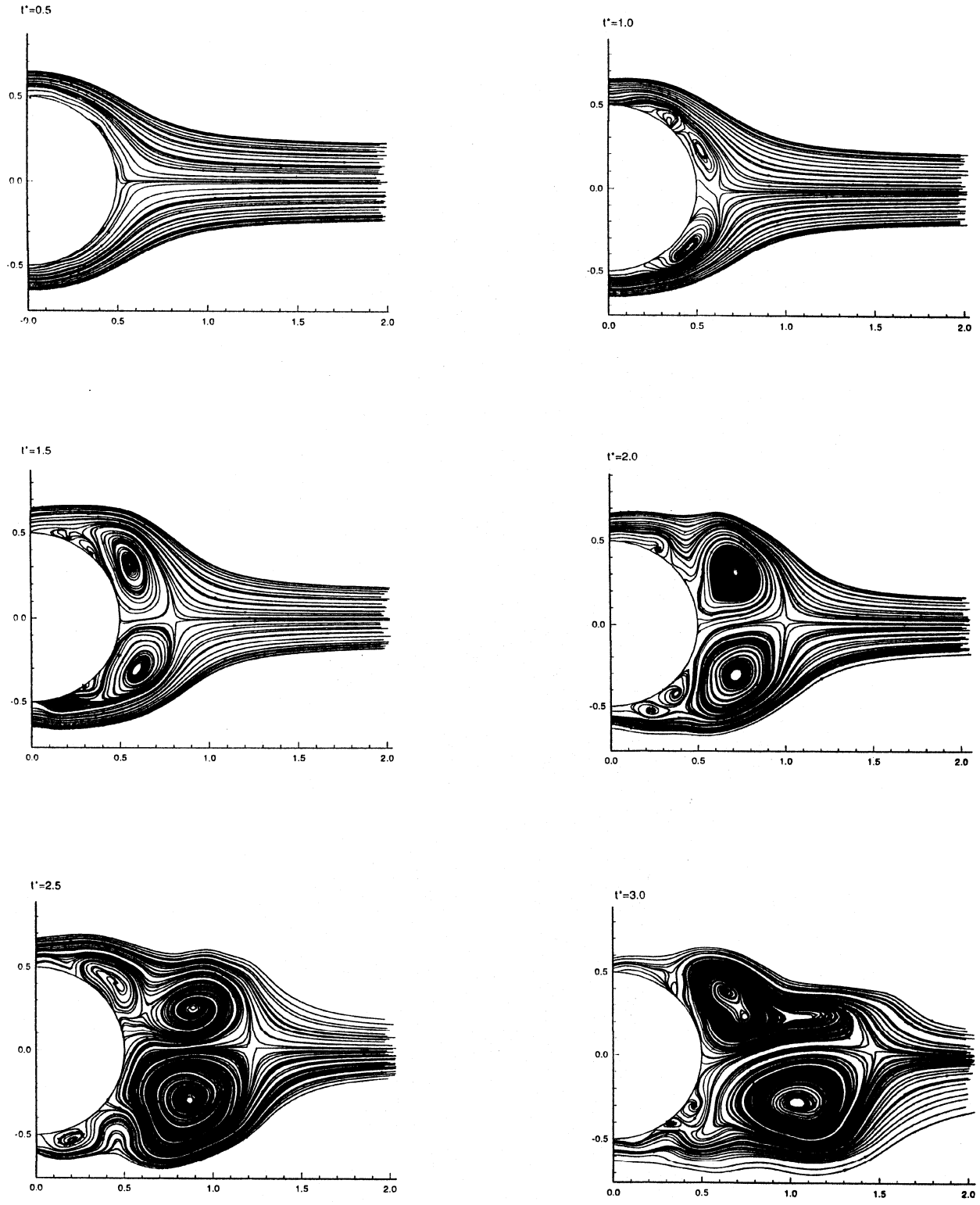

Figure 13. Streamlines for a structure during t<3.0 at Re=9500.

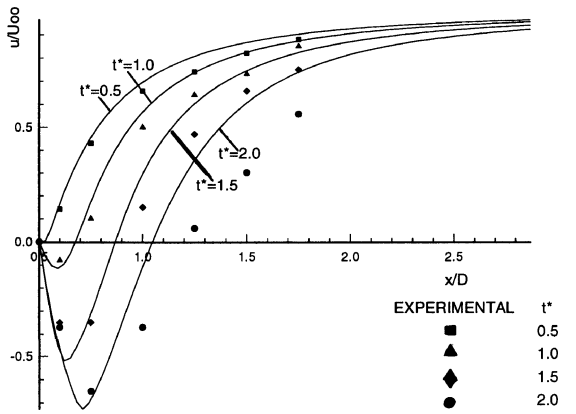

Figure 14. Radial velocity on the symmetric axis.

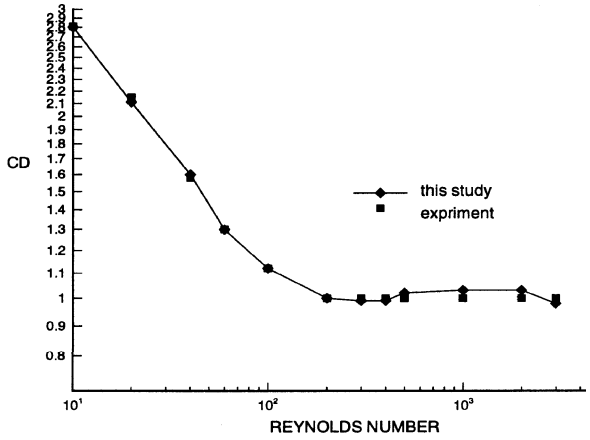

Figure 17. Variation of CD versus Re number.

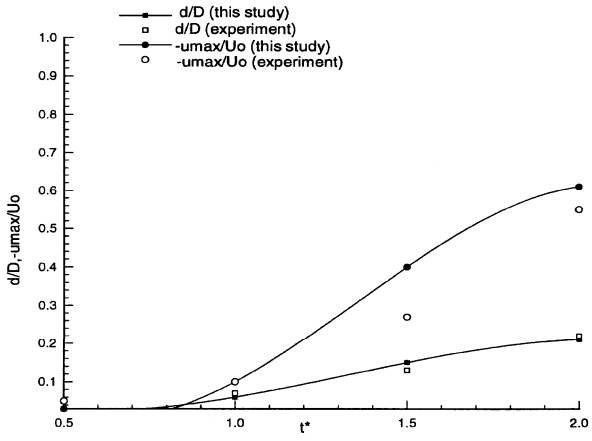

Figure 15. Location of u_{max} versus time.

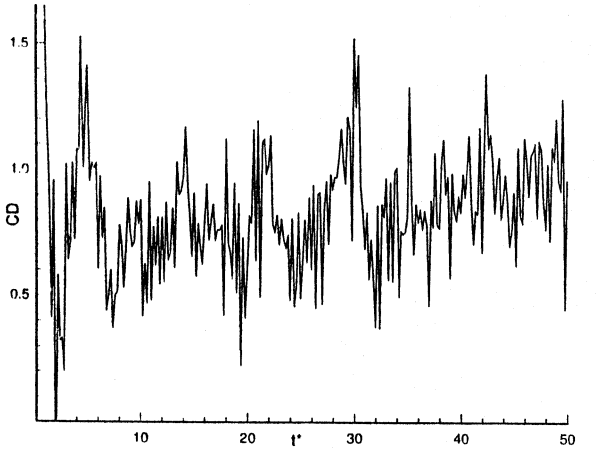

Figure 18. Drag coefficient versus time.

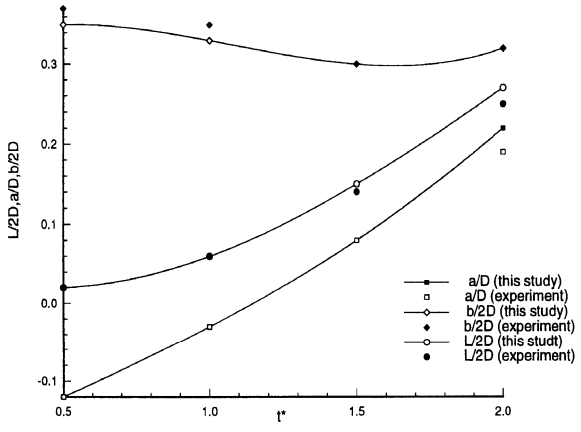

Figure 16. Length and width of eddies versus time.

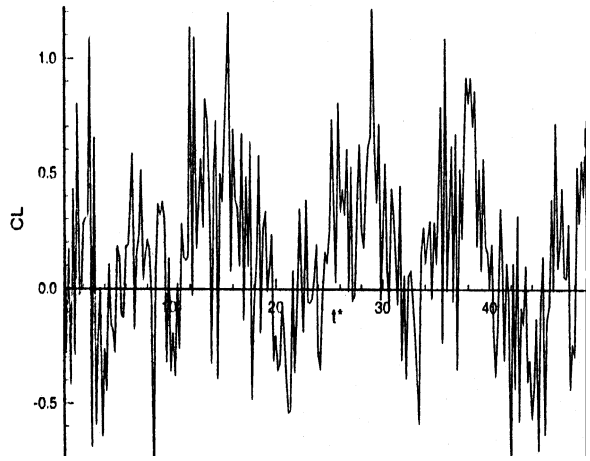

Figure 19. Lift coefficient versus time.

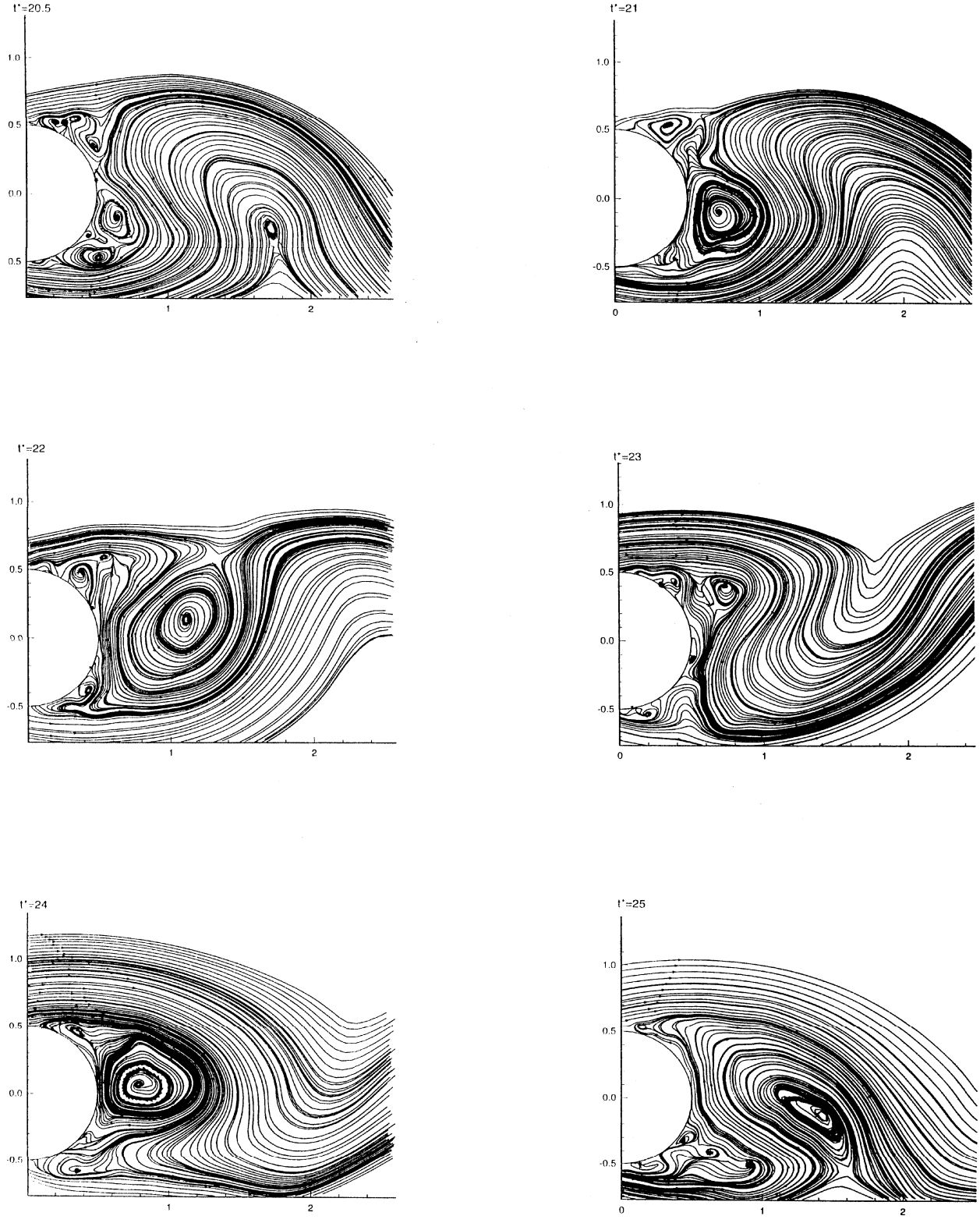

Figure 20. Streamlines for Re = 9500 at later times.

Figure 21. Positions and velocities of vortex elements downstream versus time at Re = 9500.

possible, regarding the growth of the size of the large scale structures, the two-dimensional model is not enough accurate and the three-dimensional models are needed.

6. CONCLUSION

The vortex element method has an extensive application in the numerical simulation of the turbulent flows, especially modeling the physics of the flow in the recirculating zone behind the cylinder for the initial and later times. Keeping track of the vortex elements in a Lagrangian reference, the formation, growth, convection and diffusion of the elements can very well be investigated.

The numerical results show that the variation of geometrical and physical parameters of the flow strongly depend on the Reynolds number and results have good agreements with the experimental measurements.

As the instantaneous experimental results are not available, the accuracy of these kinds of numerical results can be validated qualitatively. The comparison of the averaged based values such as separation angles, drag coefficient, lift coefficient, Strouhal number, ... with the experimental measurements proves the accuracy of the numerical results.

7. REFERENCES

1. Prandtl, W., "The Magnus Effect and Wind Powered Ships", ***Wissenschaften***, Vol. 13, (1925), 93-108.
2. Bouard, R. and Contanceau M., "The Early Stage of Development of the Wake Behind an Impulsively Started Cylinder for 40< Re< 10000", ***J. Fluid Mech.***, Vol. 101, (1980), 583-607.
3. Payne, R. B., "Calculation of Viscous Unsteady Flow Past a Circular Cylinder", ***J. Fluid Mech.***, Vol. 4, (1958), 81-86.
4. Ingham D. B., "Unsteady Separation", ***J. Comput. Phys.***, Vol. 53, (1984), 90-99.
5. Gou, T., Chew Y. T., Lou S. C. and Su M. D., "A New Numerical Method of High Reynolds Number Flow Around a Cylinder", ***Comput. Methods Appl. Mech. Engrg***, Vol. 158, (1998), 357-366.
6. Chorin, A. J., "Numerical Study of Slightly Viscous Flow", ***J. Fluid Mech.***, Vol. 57, (1973), 785-796.
7. Chorin, A. J., "Vortex Sheet Approximation of Boundary Layer", ***J. Comput. Phys.***, Vol. 27, (1978), 428-442.
8. Cheer, A. Y., "Unsteady Separated Wake Behind an Impulsively Started Cylinder in Slightly Viscous Flow", ***J. Fluid Mech.***, Vol. 201, (1989), 485-505.
9. Koumoutsakos, P. and Leonard A., "High-resolution Simulation of Flow Around an Impulsively Started Cylinder Using Vortex Methods", ***J. Fluid Mech.***, Vol. 296, (1995), 1-38.
10. Gharakhani, A. and Ghoniem A. F., "Three Dimensional Vortex Simulation of Time Dependent Incompressible Internal Viscous Flows", ***J. Comput. Phys.***, Vol. 134, (1997), 75-95.
11. Beal, J. T., "A Convergent 3-D Vortex Method with Grid Free Stretching", ***Math. Comput.***, Vol. 46(174), (1986), 401.
12. Beale, J. T. and Majda A., "Rates of Convergence for Viscous Splitting of Navier-Stokes Equation", ***Math. Comput.***, Vol. 37(156), (1981), 243.
13. Beale, J. T. and Majda A., "Vortex Method I, Convergence in Three Dimensions", ***Math. Comput.***, Vol. 39(159), (1982), 1.
14. Ghoniem, A. F. and Gagnon Y., "Vortex Simulation of Laminar Recirculating Flow", ***J. Comput. Phys.***, Vol. 68, No. 2, (1987), 346.
15. Ghoniem, A. F. and Sherman F. S., "Grid Free Simulation of Diffusion Using Random Walk Method", ***J. Comput. Phys.***, Vol. 61, (1985), 1-37.
16. Chorin, A. J. and Marseden J. E., "A Mathematical Introduction to Fluid Mechanics", Springer-Verlag., (1979).
17. Kloeden, and EcKhard Platen, "Numerical Solution of Stochastic Differential Equations", Springer Verlag., (1992).
18. Sherman, F. S., "Viscous Flow", McGraw Hill, (1990).
19. Katz, J. and Plotkin, A., "Low Speed Aerodynamics", McGrow Hill, (1991).
20. Delfani, S., "Numerical Simulation of Turbulent Flow Around the Cylinder Using Random Vortex Method", M.Sc. Thesis, Department of Mechanical Engineering, Tarbiat Modarres University, Tehran, I.R. of Iran (1998) (in Farsi).